water

MDPI

Article

Preparation of Hydrogels Based Radix Isatidis Residue Grafted with Acrylic Acid and Acrylamide for the Removal of Heavy Metals

Xiaochun Yin [1,2], Hai Zhu [2], Ting Ke [2], Yonge Gu [2], Huiyao Wang [1,*] and Pei Xu [1,*]

[1] Department of Civil Engineering, New Mexico State University, Las Cruces, NM 88003, USA
[2] School of Public Health, Gansu University of Chinese Medicine, Lanzhou 730000, China
* Correspondence: huiyao@nmsu.edu (H.W.); pxu@nmsu.edu (P.X.)

Abstract: A series of hydrogels as biosorbents to remove heavy metal ions (Pb^{2+}, Cu^{2+}, and Cd^{2+}) were prepared using Radix Isatidis residues as material grafted with acrylic acid and acrylamide. The surfaces of Radix Isatidis residue/acrylic acid-co-acrylamide (RIR/AA-co-AM), Radix Isatidis residue/polyacrylamide (RIR/PAM_3), and Radix Isatidis residue/polyacrylic acid (RIR/PAA_4) hydrogels have a sponge-like, three-dimensional, and highly microporous structure. The hydrogels all have considerable swelling properties and the swelling rate of RIR/PAA_4 is the highest at 9240%. The hydrogels all possess high adsorptivity to Pb^{2+}, Cu^{2+}, and Cd^{2+}. Under optimized conditions, the maximum adsorption capacity of RIR/AA-co-AM hydrogel is 655.4 mg/g for Pb^{2+}, 367.2 mg/g for Cd^{2+}, and 290.5 mg/g for Cu^{2+}. The maximum adsorption capacity of RIR/AA-co-AM hydrogel for Cd^{2+} and Cu^{2+} is slightly lower than that of RIR/PAA_4. In addition, the adsorption process of RIR/AA-co-AM for heavy metal ions conforms with the pseudo-second-order kinetic equation and Langmuir adsorption isotherm. Based on the microstructure analysis and adsorption kinetics, electrostatic adsorption and ion exchange are identified as the mechanisms for the hydrogels removal of heavy metal ions from water. It infers that hydrogels from Chinese herb residue can be used to effectively remove heavy metals from wastewater and improve the reutilization of Chinese herb residue.

Keywords: hydrogel; Chinese herb residue; cellulose; biosorbent; heavy metal; removal

Citation: Yin, X.; Zhu, H.; Ke, T.; Gu, Y.; Wang, H.; Xu, P. Preparation of Hydrogels Based Radix Isatidis Residue Grafted with Acrylic Acid and Acrylamide for the Removal of Heavy Metals. *Water* **2022**, *14*, 3811. https://doi.org/10.3390/w14233811

Academic Editors: Min Zheng, Jia Meng and Philip Antwi

Received: 24 October 2022
Accepted: 19 November 2022
Published: 23 November 2022

1. Introduction

With the acceleration of urbanization and the expansion of the industrial scale, water pollution caused by organic (such as pesticides [1], dyes [2], etc.), and inorganic (such as various toxic heavy metals and their oxides, acids, bases, salts, sulfides, and halides, etc.), pollutants, is becoming more and more serious [3–5]. Among pollutants, heavy metals due to their biomagnification effect through food webs, drinking water, and other ways [6], can cause seriously detrimental effects on human health when their concentrations go beyond permissible limits [7–10]. Lead, copper, and cadmium are common toxic heavy metals widely used in battery manufacturing and other industries [11]. In recent years, the pollution levels of Pb^{2+}, Cu^{2+}, and Cd^{2+} in surface water and coastal wetlands have continued to rise [6], leading to harm to the ecosystem and causing diseases to human beings [12]. For instance, persistent intake of inorganic cadmium causes irritation of the respiratory system and damages the liver, kidneys, and lungs in humans via the consumption of drinking water [13]. Lead accumulation in the food chain shows a negative impact on human health, such as damage to the central nervous system, fetal brain, kidney, reproductive system, liver, basic cellular processes, and causes diseases (such as anemia, nephrite syndrome, hepatitis) [14]. Therefore, it is urgent and necessary to remove toxic heavy metals from contaminated water.

Recently, biosorbents have attracted more attention due to their high removal efficiency, low cost, no chemical sediment, and easy availability [15,16]. However, preparing biosorbents with high adsorption capacity and fast adsorption rate needs intensive study [17,18]. At present, biosorbents from natural by-product materials (such as cellulose [19], chitosan [20], keratin [21,22], zeolite and clay [23]), are potential options because of their widely avaiable resources, eco-friendliness, biocompatibility, and low cost. Cellulose, a natural macromolecular compound and one of the most abundant renewable resources in nature, mainly comes from plants sources such as Chinese herbal residue [24], bamboo [25], cotton straw [26–28], sawdust [29], nutshell [30], and Napier grass [31], which has the characteristics of high toughness, biocompatibility, biodegradability [32], and excellent adsorptivity for heavy metals. Furthermore, several studies have reported the excellent performance of biosorbents-based cellulose for the removal of heavy metal ions (such as mercury, lead, cadmium, and copper) in wastewater [6,10,15]. Therefore, cellulose-based biosorbents have excellent prospects for the removal of heavy metals from wastewater.

Chinese herb residue-based biosorbent is a potential adsorbent due to being rich in cellulose, large tonnage, and easy availability [33]. According to statistics, the annual discharge of Chinese herb residues in the country is as high as 650,000 tons [34], which will pollute the environment and groundwater because it is highly susceptible to rot if it is not timely and properly treated [35]. Many researches have studied the utilization of Chinese herb residue for protecting the environment (such as removing dyes [36] and heavy metals [37] from wastewater). In addition, according to our previous study, Radix Isatidis residue (RIR) can remove Cu^{2+} from the water to some degree, but it was found that its adsorption capacity was extremely low (16.5 mg/g). Additionally, our team previously prepared a series of biosorbents to remove Cu^{2+} in water by chemically modified licorice residue (LR) [16] and RIR, but the adsorption capacity of modified RIR (31.0 mg/g) was low because cellulose was embedded in lignocellulose and its functional groups were difficult to expose, which made Chinese herb residues sparingly soluble in water. Although the researchers had taken advantage of the cellulose in Chinese herb residues to remove contaminants from wastewater, the cellulose mostly is wrapped in lignin and is compact, resulting in low adsorption capacities and rates [38]. Therefore, developing the methods to effectively dissolve the cellulose, remove lignin in Chinese herb residues, and improve the adsorption efficiency has become an essential approach. To overcome these challenges, our team previously adopted an alkaline solution to dissolve them at a low temperature (−20 °C) and using a microwave to achieve their complete dissolution, supporting a possible way to improve the utilization and further application of Chinese herb residues.

In recent years, as a bio-adsorbent for heavy metal removal, hydrogels have entered people's vision due to their advantages of simple synthesis, convenient application, and wide selection of raw materials [39,40]. Unlike other adsorbents, hydrogels, a 3D network structure composed of hydrophilic polymer chains crosslinked either physically, chemically, or via polymerization, adsorb heavy metals in a three-dimensional and highly porous network [41]. Hydrogels can retain a large amount of water in a swollen state within their network from surface tension and capillary forces [42], leading to a high adsorption efficiency [43]. The adsorption or desorption of hydrogels for heavy metals is mainly due to the surface chemistry and presence of hydrophilic functional groups (−OH, −COOH, $-CONH_2$, and $-SO_3H$, etc.), which act as a complexing agent for heavy metals removal from wastewater [44,45]. Moreover, hydrogels can be modified with the addition of new functional metal absorption capacities or the preparation of composites with natural or synthetic sources such as cellulose [46] to enhance heavy metal adsorption capacities [47].

As for the material, hydrogel can be produced either from natural or synthetic polymers. However, natural-based polymer hydrogel is more prominent due to its low cost, good biocompatibility, and biodegradability. Chinese herb residue containing a large amount of cellulose is a promising natural material for preparing hydrogels for removing heavy metals from wastewater. To date, there are limited studies that used Chinese herb residue as raw materials to synthesize hydrogel. Using Chinese herb residue as a source to

prepare hydrogel is not only a promising method to remove heavy metals from wastewater, but also a sustainable approach to improve the reutilization value of Chinese herb residue.

In this paper, the dissolved Radix Isatidis residue (RIR) was used as a raw material, acrylamide (AM) and acrylic acid (AA) were functional monomers with numerous functional groups ($-CONH_2$, $-COOH$), N,N methylene bisacrylamide (MBA) and amine persulfate were crosslinking agent and initiator, respectively. A series of hydrogels used as biosorbents to remove heavy metals from wastewater were synthesized through free radical polymerization. The prepared hydrogels were characterized by scanning electron microscopy (SEM) and Fourier transform infrared spectroscopy (FTIR). The adsorption capacities of the hydrogel adsorbents were studied by the static adsorption test, and the effect of pH of the solution, adsorption time, adsorbent dosage, and initial concentration of Cu^{2+}, Pb^{2+}, and Cd^{2+} were investigated. The kinetic model and the isotherm model were used to analyze the adsorption kinetics and adsorption capacity. Lastly, the adsorption mechanism of hydrogel for the removal of heavy metals was discussed. In this study, a series of biosorbents with excellent adsorption properties were synthesized using Chinese herb residues at room temperature. This low-cost and convenient synthesis method supports the reutilization of Chinese herb residues, the development of biosorbents, and more importantly the reduction of environmental pollution stress.

2. Experimental

2.1. Materials

Radix isatidis was obtained from Huiren Tang Pharmacy (Lanzhou, China). Urea (CH_4N_2O) were purchased from Yantai Shuangshuang Chemical Co., LTD (Yantai, China). Sodium hydroxide (NaOH), AM, AA and N,N-methylene bisacrylamide (MBA) were purchased from Tianjin Damao Chemical Reagent Factory (Tianjin, China). Ethanol absolute (C_2H_6O) and ammonium persulfate (APS) were purchased from Tianjin Best Chemical Co., LTD. (Tianjin, China). Lead nitrate ($Pb(NO_3)_2$), hydrated copper sulfate ($CuSO_4 \bullet 5H_2O$), and cadmium chloride hydrate ($CdCl_2 \bullet 2\ 1/2H_2O$) were acquired from Tianjin Kermel Chemical Reagent Co., LTD. (Tianjin, China). All other chemical reagents were of analytical grade and used directly without further purification.

2.2. Pretreatment of Radix Isatidis Residue (RIR)

The RIR was washed with distilled water, boiled three times to remove the active ingredients from RIR, and dried at 50 °C. Firstly, the dried RIR was modified with diluted NaOH (1 mol/L) for 8 h, named as RIR-NaOH. After drying and grinding, RIR-NaOH was sieved with a 200-mesh screen (Figure 1a). An amount of 7 g of sodium hydroxide and 12 g of urea were dissolved in 81 mL of distilled water, named as the alkaline urea solution. Then, the RIR-NaOH powder was dispersed in the alkali–urea solution at room temperature with magnetic stirring 2 h (200 rmp), next this mixture was frozen at −20 °C for 8 h, and then thawed and stirred at 0 °C for 2 h; this process was repeated twice. Lastly, microwave radiated the above mixture for 20 min, the mixture was centrifuged for 5 min at 4000 rpm, and the supernatant was added with 1M HCl solution to neutral pH and stored at 4 °C (Figure 1b).

2.3. Preparation of Hydrogels

The RIR-NaOH supernatant was stirred at room temperature for 15 min, and AA (3 mL), AM (2 g), and MBA (0.2 g) were added. Then, the appropriate amount of APS solution was added to generate hydroxyl radicals. Lastly, the mixture solution was stirred for 1 min and maintained for 20 min to generate hydrogel at room temperature. The reaction scheme is illustrated in Figure 2. After the reaction, the sample was washed with absolute ethanol to remove unreacted reagents and by-products. Next, the hydrogel was soaked in distilled water and changed water twice, which was lyophilized to produce the final biosorbent (named RIR/AA-co-AM). At the same time, a series of hydrogels were fabricated by introducing AA (2 mL, 3 mL, 4 mL) or AM (1 g, 2 g, 3 g) with the same method

as mentioned above, named as RIR/PAA_2, RIR/PAA_3, RIR/PAA_4, RIR/PAM_1, RIR/PAM_2, and RIR/PAM_3, respectively. Because RIR/PAA_4 and RIR/PAM_3 have better physical properties than other hydrogels of the same series, only RIR/PAA_4 and RIR/PAM_3 were compared with RIR/AA-co-AM in the following study.

(**a**) (**b**)

Figure 1. RIR powder (**a**); the supernatant solution of RIR-NaOH (**b**).

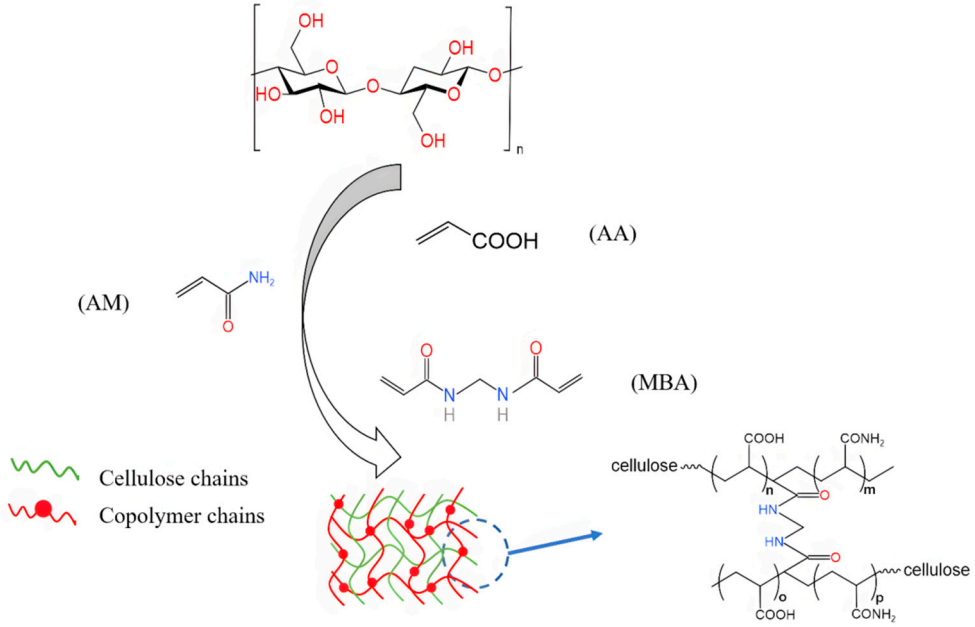

Figure 2. The synthesis scheme of RIR/AA-co-AM hydrogel.

2.4. Characterization

The surface morphologies and structures of the dried hydrogels were observed using scanning electron microscopy (SEM; JSM-6701F, JEOL, Tokyo, Japan) with an accelerating voltage of 20 kV. Hydrogels were mounted on aluminum sample holders with double-sided tape and coated with a thin layer of gold.

The structures of RIR-NaOH, RIR/AA-co-AM, RIR/PAA_4, and RIR/PAM_3 were characterized with Fourier transform infrared spectrometer (FTIR, Nicolet Nexus, Waltham, MA, USA). The hydrogels were dried and ground into potassium bromide tablets containing 1% of the sample, and spectra were collected at wavenumbers from 400 cm^{-1} to 4000 cm^{-1}.

2.5. Swelling Experiments

In order to characterize the swelling behavior of hydrogels, 3 pieces of dry hydrogels (50 mg) were immersed into 50 mL DI water at room temperature (25 °C). After swelling for 24 h and reaching equilibrium, the weight of swollen hydrogels was measured. The swelling ratio (S_w) of the hydrogels was calculated according to Equation (1) [48]:

$$S_w(\%) = \frac{W_s - W_d}{W_d} \times 100 \quad (1)$$

where W_d (g) is the weight of dry hydrogels; W_s (g) is the weight of swollen hydrogels at equilibrium.

2.6. Adsorption Experiments

An amount of 0.02 g of hydrogel samples was added to the colorimetric tube containing 25 mL of the heavy metal aqueous solution, and the adsorption experiment of Pb^{2+}, Cd^{2+}, and Cu^{2+} on RIR/AA-co-AM, RIR/PAA_4, and RIR/PAM_3 were studied. The cuvettes were sealed and stirred in a thermostatic shaker (stirring at 120 rpm) at room temperature, and the pH of the solutions was adjusted by adding appropriate HCl and NaOH solutions. The effect of pH on metal ion adsorption between 1.0 and 5.0 was investigated. In adsorption kinetic experiments, the contact time was 0.25–8 h. In the adsorption isotherm experiment, the metal ion concentrations were between 100 and 1000 mg/L. After adsorption, the residual concentration of heavy metal ions was determined using atomic absorption spectroscopy (PerkinElmer, PinAAcle 900 T, Waltham, MA, USA).

The adsorption capacity (q_e, mg/g) and heavy metal ions adsorption capacity (q_t, mg/g) of the hydrogel at equilibrium were determined by the following equations [44].

$$q_e = \frac{(C_0 - C_e)V}{W} \quad (2)$$

$$q_t = \frac{(C_0 - C_t)V}{W} \quad (3)$$

where q_e (mg/g) is the equilibrium adsorption capacity, q_t (mg/g) is the adsorption capacity at a specific time, C_0 (mg/L) is the initial concentration, C_e (mg/L) is the equilibrium concentration, and C_t (mg/L) is the concentration of heavy metal solution at time t (h), V (mL) the volume of heavy metal ion solution, and W (mg) is the amount of dry hydrogel.

3. Results and Discussion

3.1. Structure Characterization and Analysis of Hydrogels

3.1.1. Photos of RIR/AA-co-AM Hydrogel

The morphology of RIR/AA-co-AM was photographed as shown in Figure 3. The prepared hydrogel looks like a jelly-like solid (a) maintained high water capacity due to its high porosity structure [49]. After soaking in anhydrous ethanol, the gel lost a part of the water, becoming tougher and more elastic (b). When soaked in distilled water, the gel absorbed water and swelled rapidly (c). The lyophilized RIR/AA-co-AM showed a loose and porous three-dimensional network shape, which was beneficial to provide more sites for ion adsorption (d). Compared with the hydrogel introduced with acrylic monomer, the hydrogel obtained by cross-linking polymerization of acrylamide and acrylic acid has greatly improved elasticity and toughness and has better mechanical properties. It is easy to recycle in future experiments, thereby reducing secondary pollution.

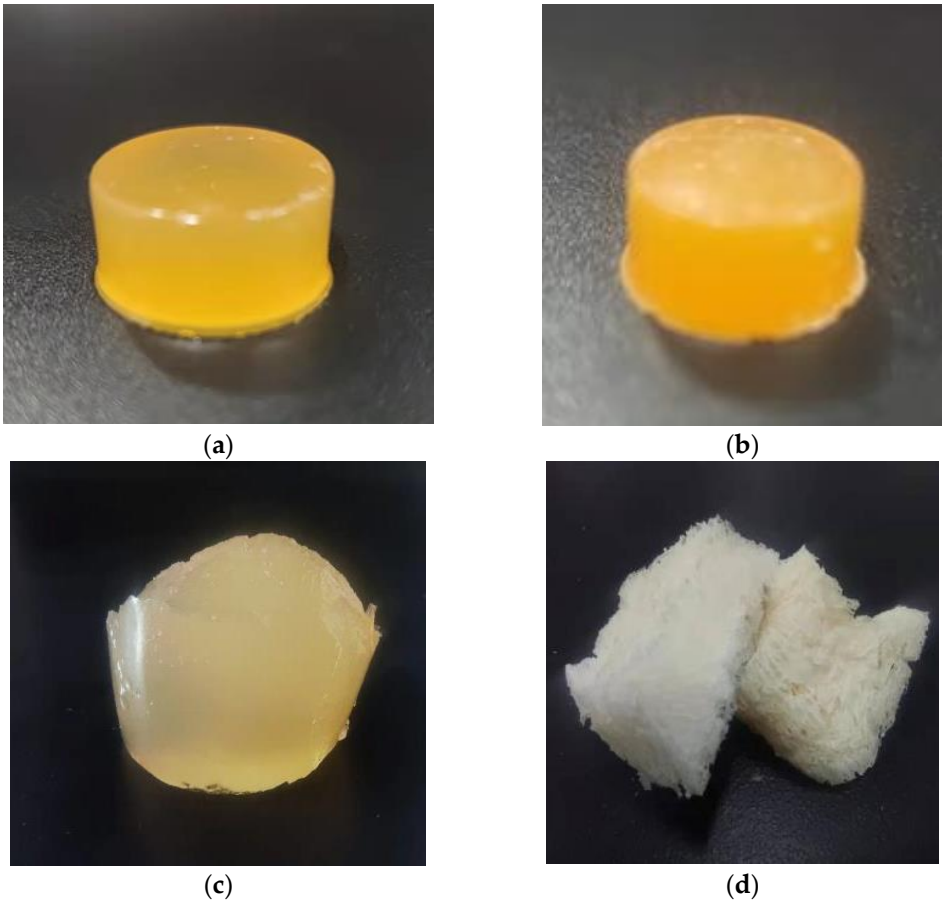

Figure 3. The photos of RIR/AA-co-AM hydrogel. Prepared RIR/AA-co-AM hydrogel (**a**); After ethanol dehydration (**b**); After soaking in DI water for 24 h (**c**); After freeze drying (**d**).

3.1.2. SEM

The surface morphology of RIR, RIR-NaOH, RIR/PAM_3, RIR/PAA_4, and RIR/AA-co-AM was analyzed by SEM, as shown in Figure 4. The RIR structure was relatively loose with few regular pores. Although RIR-NaOH has a few pores, they were larger than 10 µm which made the pollutants easy in and out, leading to a low adsorption capacity. Based on the structure of RIR and RIR-NaOH, their adsorption capacities for heavy metals were lower because cellulose is wrapped in lignin and is compact, resulting in low adsorption capacities and rates [46]. The porosity of hydrogel is a key factor attributed to its adsorption capacity [50]. Compared with RIR and RIR-NaOH, the hydrogels of RIR/AA-co-AM, RIR/PAM_3, and RIR/PAA_4 have sponge-like, three-dimensional, and highly microporous surface morphology. Among hydrogels, RIR/AA-co-AM has a regular porous and rough structure that significantly differs from RIR/PAM_3 and RIR/PAA_4 hydrogel. The average pore size of RIR/AA-co-AM in diameter is about 3 µm, slightly larger than RIR/PAM_3 and RIR/PAA_4, which can provide more adsorption sites for heavy metal ions and improve the overall adsorption performance. The hydrogel RIR/PAA_4 has a highly porous structure, leading to a higher adsorption capacity than RIR/PAM_3. The main reason that the pores developed in the hydrogel would improve the adsorption performance is that the pores can permit guest molecules such as water and heavy metals to move across the composite structure [51].

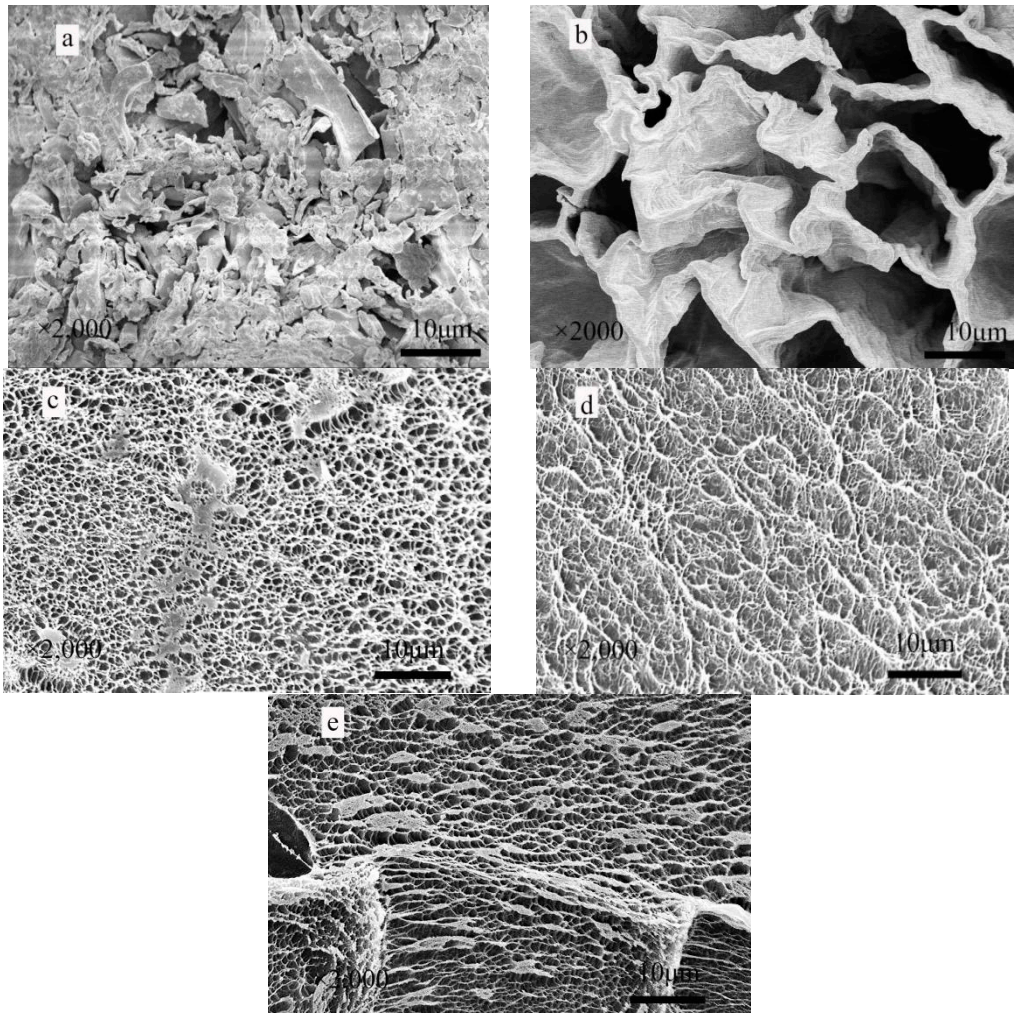

Figure 4. SEM images of RIR (**a**), RIR-NaOH (**b**), RIR/PAM_3 (**c**), RIR/PAA_4 (**d**) and RIR/AA-co-AM (**e**).

3.1.3. FTIR Analysis

Various functional groups in hydrogels were determined by FTIR, as shown in Figure 5. The absorption band around 3430 cm^{-1} is related to the O-H bond [16], the sharp peak at 2927 cm^{-1} is related to the C_{sp3}- stretching vibration [52], the peak at 1623 cm^{-1} is the stretching of the C-N bond, the peak at 1413 cm^{-1} is related to the stretching vibration of the -CO- bond in the phenyl hydroxyl group in lignin, the peak at 1314 cm^{-1} is the C-N absorption band (amide III band), the peaks at 1158 cm^{-1} are attributed to the stretching vibration of the ester bond in the cellulose ester group [16], the peak at 1030 cm^{-1} is attributed to the bending vibration of the hydroxyl group [53], and the characteristic peaks of cellulose still exist in RIR/AA-co-AM, RIR/PAA_4, and RIR/PAM_3 hydrogels. The peak at 2852 cm^{-1} is the characteristic absorption peak of methylene symmetry stretching vibration, and 1454 cm^{-1} is the characteristic absorption peak of methylene deformation [54], the vibration peak of C=O at 1561 cm^{-1}, the absorption peak at 1119 cm^{-1} is related to the C-N stretching vibration, these characteristic peaks are all from polyacrylamide and polyacrylic acid. It can be seen that AA and AM were successfully introduced onto RIR-NaOH by graft copolymerization.

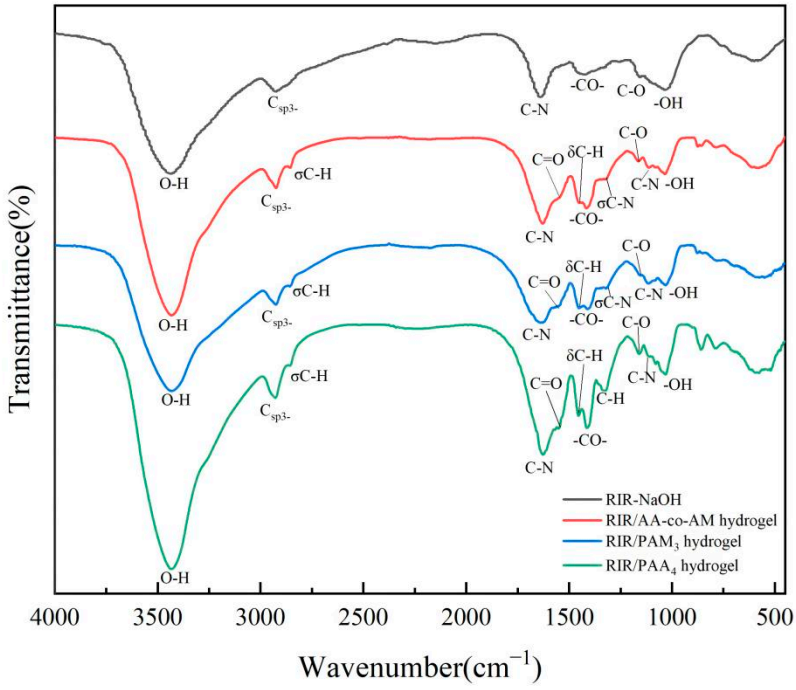

Figure 5. FTIR spectra of RIR-NaOH, RIR/AA-co-AM, RIR/PAM_3 and RIR/PAA_4.

3.2. Swelling Ratio of Hydrogels

Figure 6 shows the results of the swelling properties of different hydrogels. RIR/PAA_4 and RIR/AA-co-AM had the highest swelling rate (9240%) due to numerous hydrophilic functional groups (e.g., –OH, −COOH, $-NH_2$), which enable the adsorption and retention of a large volume of water. After introducing $CONH_2$, the swelling ratio (9064%) of RIR/AA-co-AM and RIR/PAM_3 were all lower than that of RIR/PAA_4, and RIR/PAM_3 had the lowest swelling rate (4024%) because the hygroscopicity of COOH is higher than that of $CONH_2$ on the surface of RIR/AA-co-AM and RIR/PAM_3 [55]. Although RIR/PAA_4 has the best swelling ratio among the three hydrogels, it could not maintain its form in the process of adsorption.

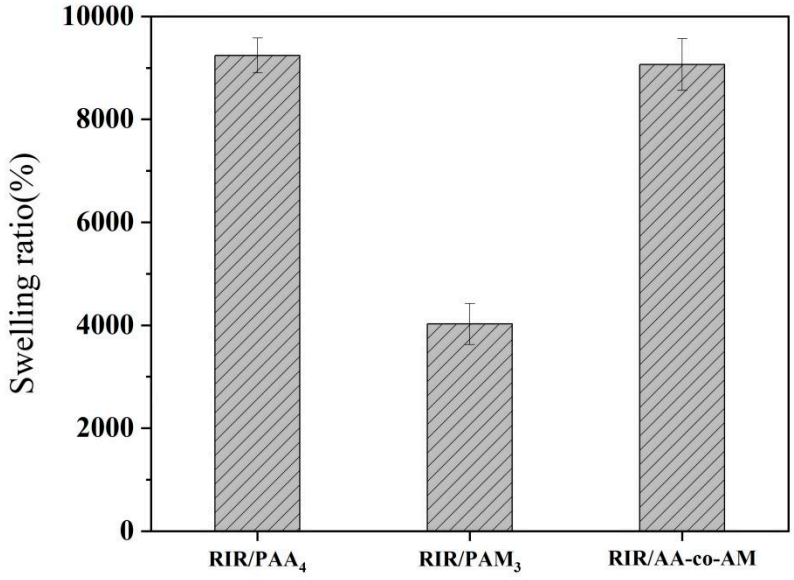

Figure 6. The swelling ratio of RIR/PAA_4, RIR/PAM_3, and RIR/AA-co-AM.

3.3. Adsorption of RIR/AA-co-AM

3.3.1. Effect of pH on Adsorption

The effect of pH on adsorption is shown in Figure 7. In this experiment, pH is a critical parameter for the adsorption process that can change the chelating ability of adsorbents by affecting their swelling ability and interactions between adsorbents and ions [56]. The adsorption capacity of RIR/AA-co-AM hydrogel for Pb^{2+}, Cd^{2+}, and Cu^{2+} increased with the solution pH and remained balanced at pH 3 (Figure 7a). This trend could be explained by the changes in active sites on the hydrogel surface [57]. Here, the hydroxyl, -$CONH_2$, and -COOH were the main adsorption groups. When the solution pH was below 1, the adsorption capacity of RIR/AA-co-AM to heavy metals was close to 0 mg/g, while the adsorption capacity of the hydrogel increased rapidly when pH increased in the range of 1–3. It was mainly because when pH was lower than 1, there was a competition between hydrogen ions and metal ions to bound active sites on the surface of the hydrogels. In addition, the active groups -OH, -$CONH_2$, and -COOH were protonated by hydrogen ions, reducing the number of adsorbing sites available for metal ions uptake. Furthermore, a large amount of H^+ in the solution can compete with metal ions via the ion-exchange reaction. As the pH increased, the number of positively charged surface active sites decreased, which lowered the electrostatic repulsion between the positively charged heavy metal ions and the surface of the adsorbent. At pH 3, the adsorption capacity of RIR/AA-co-AM to Pb^{2+}, Cd^{2+}, and Cu^{2+} reached the maximum. Therefore, the use of hydrogel to adsorb heavy metal ions is based on their electrostatic interactions and ion exchange and does not require high alkalinity [58]. At higher pH (pH > 5.5), the number of adsorption sites is expected to increase because there are more basic amino groups. However, in this pH range, Pb^{2+}, Cd^{2+}, and Cu^{2+} can precipitate as insoluble hydroxides [59], possibly leading to an inaccurate interpretation of the obtained results. Therefore, a pH of 3.0 was selected as the initial pH for RIR/AA-co-AM to adsorb Pb^{2+}, Cd^{2+}, and Cu^{2+} solutions for the following adsorption experiments.

From Figure 7b–d, RIR/PAA_4 and RIR/PAM_3 reached the maximum adsorption to heavy metals at pH 4. At pH 3, the adsorption capacity of RIR/AA-co-AM for Pb^{2+} could reach 655.38 mg/g at equilibrium, which was higher than those of Cd^{2+} (219.13 mg/g) and Cu^{2+} (242.79 mg/g). It might be because numerous functional groups -$CONH_2$ [60] and -COOH [61] on RIR/AA-co-AM surface have more selective adsorption to Pb^{2+}. Figure 7c,d show that the RIR/AA-co-AM also had a better adsorption effect on Cu^{2+} and Cd^{2+} ions, which could reach 242.79 mg/g and 260.69 mg/g, respectively. The high uptake of Cu^{2+} and Cd^{2+} of RIR/PAA_4 may be attributed to the electrostatic attraction between the Cu^{2+} and Cd^{2+} ions and the negatively charged binding sites, as ligands such as carboxyl, hydroxyl, and amino groups were free to facilitate interactions with metal cations [62]. However, RIR/AA-co-AM had a better adsorption effect on Cu^{2+} and Cd^{2+} ions which could reach to 284 mg/g and 303 mg/g. It might because the electrostatic interaction between RIR/PAA_4 and Cu^{2+} or Cd^{2+} ions is stronger than RIR/AA-co-AM and RIR/PAM_3 at pH 4. In the following study, pH 4 was chosen as the appropriate pH for RIR/PAA_4 and RIR/PAM_3 to remove heavy metals ions.

3.3.2. Effect of Contact Time on Adsorption

Figure 8a elucidates the effect of contact time on the adsorption of heavy metal ions to the hydrogels. The adsorption capacity of RIR/AA-co-AM increased with contact time and reached equilibrium at 16 h for Pb^{2+}, 2 h for Cu^{2+}, and Cd^{2+}. For Cu^{2+} and Cd^{2+}, the active sites on the surface of hydrogel were decreased and saturated, reaching the adsorption equilibrium. Additionally, the adsorption capacity of the RIR/AA-co-AM for Pb^{2+} could reach more than 350 mg/g within 2 h. RIR/AA-co-AM had fast adsorption rate and high adsorption capacity for Pb^{2+} than Cu^{2+} and Cd^{2+}. Furthermore, in Figure 8b, the removal of Pb^{2+} was mainly carried out in the first stage (2 h), and the hydrogel RIR/AA-co-AM has the fastest adsorption rate. The reason might be because the active sites (-COOH, -$CONH_2$) on the surface of RIR/AA-co-AM were more than those of RIR/PAA_4 and RIR/PAM_3

hydrogels. The adsorption capacity of RIR/AA-co-AM continued to rise to 639.46 m/g in the next 12 h (Figure 8e).

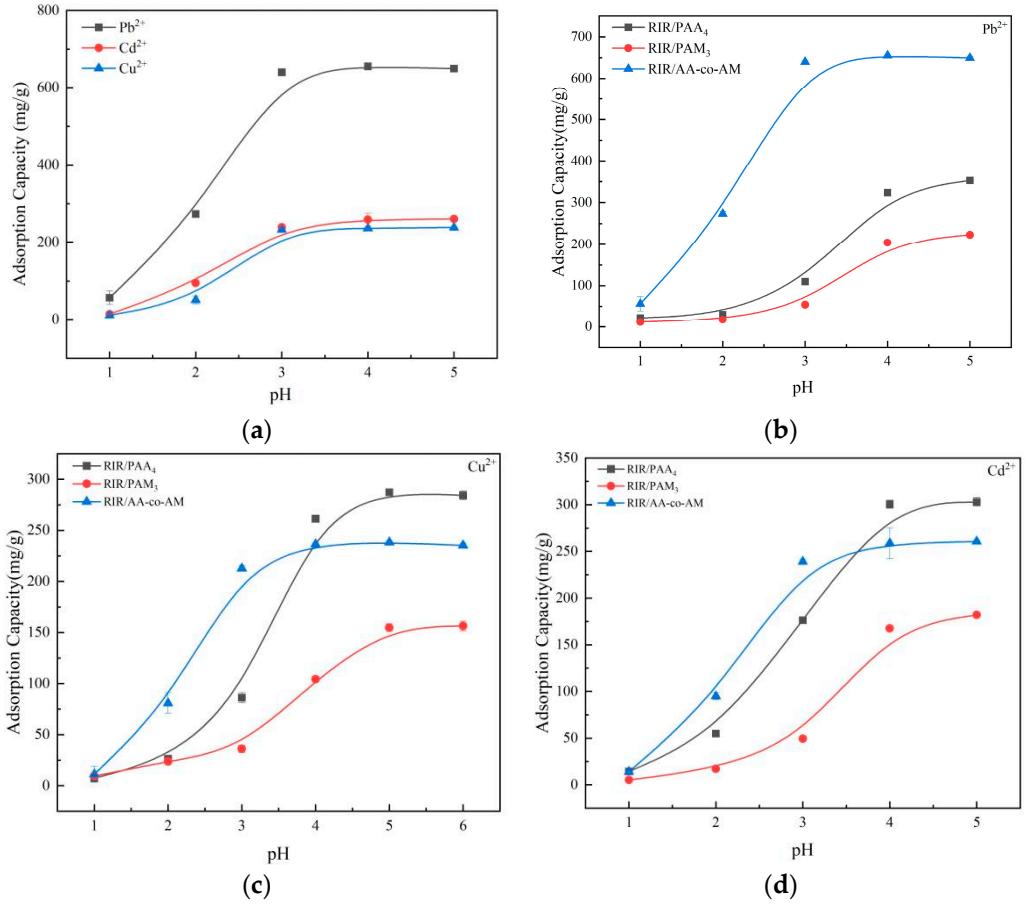

Figure 7. Effects of pH of Pb^{2+}, Cd^{2+}, and Cu^{2+} adsorption. Adsorption conditions were at absorbent = 0.02 g, T = 25 °C, and t = 8 h. Adsorption capacity of RIR/AA-co-AM for Pb^{2+}, Cd^{2+}, and Cu^{2+} (**a**); Adsorption capacity of three hydrogels for Pb^{2+} (**b**); Adsorption capacity of three hydrogels for Cu^{2+} (**c**); Adsorption capacity of three hydrogels for Cd^{2+} (**d**).

Figure 7c,d depict the adsorption effect of three hydrogels on Cu^{2+} and Cd^{2+} under different contact times. The removal rate of RIR/AA-co-AM for Cu^{2+} and Cd^{2+} was faster than RIR/PAA_4 and RIR/PAM_3, but the maximum adsorption capacity of RIR/PAA_4 (278.5 mg/g) for Cu^{2+} was higher than RIR/AA-co-AM (240.5 mg/g) and RIR/PAM_3 (121.25 mg/g) hydrogels. Moreover, the RIR/PAA_4 had the best adsorption effect on Cd^{2+} ions which could reach 376.25 mg/g. This may be because RIR/PAA_4 could swell rapidly, thereby enhancing the adsorption capacity for Cu^{2+} and Cd^{2+}. The removal of three heavy metal ions mainly occurred in the first stage when the adsorption sites were most bound with the metal ions, which may gather near the active sites (-OH, -$CONH_2$, and -COOH), that is, the adsorption saturation state of the hydrogels.

3.3.3. Effect of Initial Ion Concentration on Adsorption

Figure 9a illustrates the effect of initial concentration on the adsorption of heavy metal ions by the RIR/AA-co-AM. The adsorption capacity increased with the increases in initial concentration, and Pb^{2+} and Cd^{2+} reached equilibrium at 600 mg/L, and Cu^{2+} reached equilibrium at 300 mg/L. In a fixed solution volume and adsorbent mass, the number of Pb^{2+}, Cd^{2+}, and Cu^{2+} proliferated when the initial concentration in wastewater increased [63]. Consequently, more Pb^{2+}, Cd^{2+}, and Cu^{2+} bound to the active sites of RIR/AA-co-AM, thus accelerating the diffusion of heavy metals onto RIR/AA-co-AM sites

due to the increase in driving force of concentration gradient, resulting in higher adsorption capacities [64]. However, with a further increase in the initial concentration, the adsorption capacity remained at the maximum levels. The following explanation was made: at low pollutant concentration, the ratio of an initial number of moles of pollutant ions to the accessible sites of hydrogels is large, which causes higher adsorption capacity. On the other hand, at higher pollutant concentrations, the number of available adsorbent sites becomes fewer, resulting in a decrease in pollutant removal efficiency [65,66].

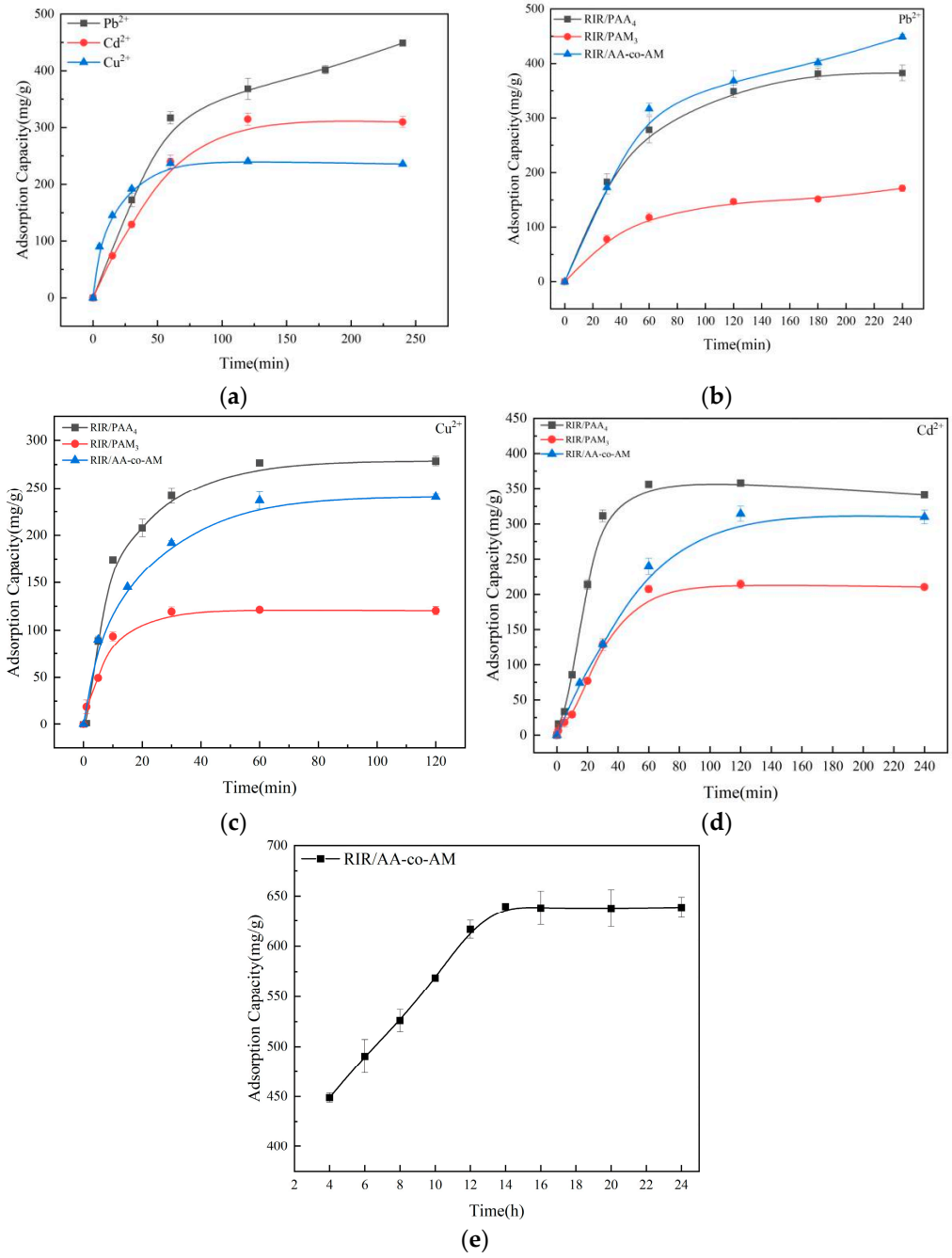

Figure 8. Effects of contact time for Pb^{2+}, Cu^{2+}, and Cd^{2+} on hydrogels. Adsorption conditions were at absorbent = 0.02 g, T = 25 °C and pH = 3 for RIR/AA-co-AM, pH=4 for RIR/PAA_4 and RIR/PAM_3. Adsorption capacity of RIR/AA-co-AM for Pb^{2+}, Cd^{2+}, and Cu^{2+} (**a**); Adsorption capacity of three hydrogels for Pb^{2+} (**b**); Adsorption capacity of three hydrogels for Cu^{2+} (**c**); Adsorption capacity of three hydrogels for Cd^{2+} (**d**); Adsorption capacity of RIR/AA-co-AM for Pb^{2+} after 4 h (**e**).

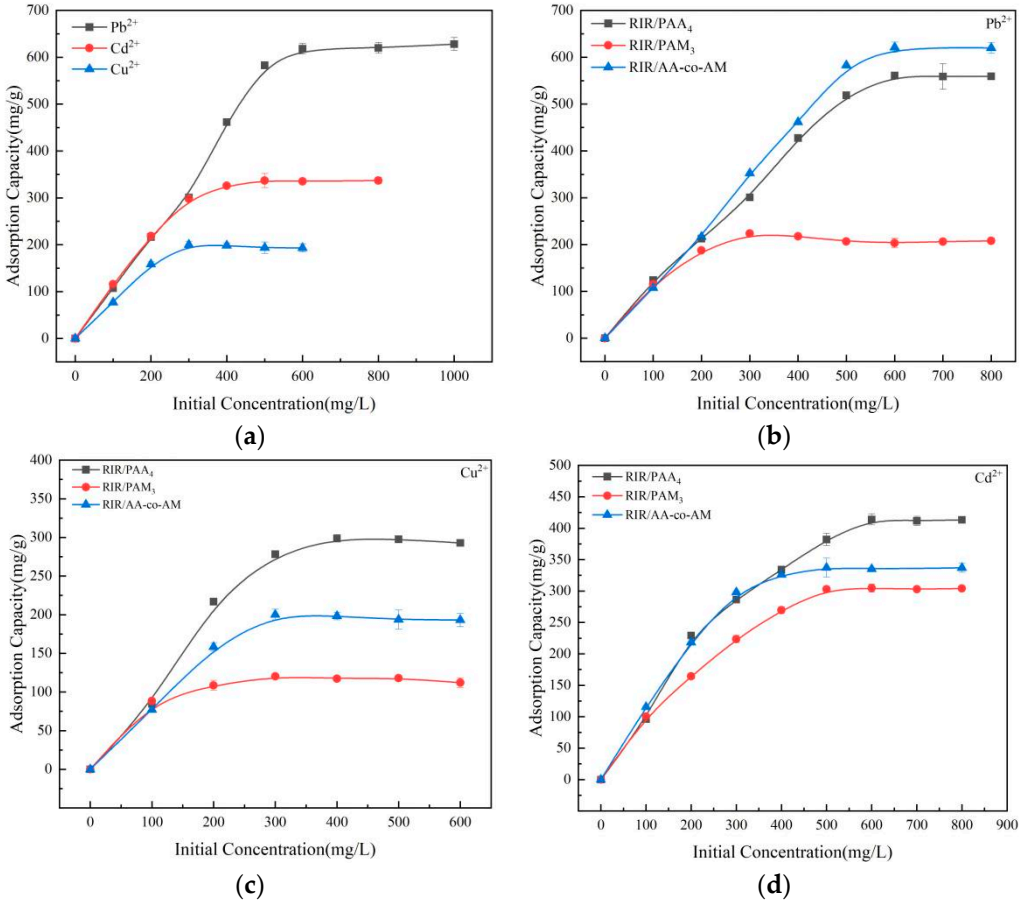

Figure 9. Effect of initial concentration on Pb^{2+}, Cu^{2+}, and Cd^{2+} adsorption. Adsorption conditions were at absorbent = 0.02 g, T = 25 °C, pH = 3 for RIR/AA-co-AM, pH = 4 for RIR/PAA_4 and RIR/PAM_3, and t = 8 h. Adsorption capacity of RIR/AA-co-AM for Pb^{2+}, Cd^{2+}, and Cu^{2+} (**a**); Adsorption capacity of three hydrogels for Pb^{2+} (**b**); Adsorption capacity of three hydrogels for Cu^{2+} (**c**); Adsorption capacity of three hydrogels for Cd^{2+} (**d**).

Figure 9b–d describe the adsorption effects of three hydrogels on three metal ions under different initial concentration solutions. With the increase in the initial ion concentration of the solution, the adsorption capacity increased, and finally tended to equilibrium. From Figure 9b, at the same initial concentration, the adsorption capacity of RIR/AA-co-AM for Pb^{2+} could reach 618 mg/g, which was higher than those of Cd^{2+} and Cu^{2+}. The possible reason for RIR/AA-co-AM had high adsorption ability for heavy metals is mainly because the hydrogels were highly porous and comprised of numerous hydrophilic functional groups (e.g., –OH, $-COOH$, $-NH_2$, and $-CONH_2$), that enabled the adsorption and retention of a large volume of water during the treatment process and eventually caused up to the complete removal and recovery of aqueous heavy metals [67]. Figure 9c,d show that the RIR/AA-co-AM also had a better adsorption effect on Cu^{2+} and Cd^{2+} ions, which could reach 212.17 mg/g and 337.16 mg/g, respectively. However, the adsorption capacity of RIR/PAA_4 for Cu^{2+} (308 mg/g) and Cd^{2+} (414 mg/g) was higher than RIR/AA-co-AM, this might be the reason that RIR/PAA_4 had stronger electrostatic adsorbability for Cu^2 and Cd^{2+} ions than that of RIR/AA-co-AM and RIR/PAM_3.

After the adsorption reaches equilibrium, there was a plateau state for the adsorption capacity of three adsorbents. This was because when the initial concentration was low, the active sites of adsorption were not saturated. As the concentration increased, the driving force for adsorption increased, which led to an increase in adsorption capacity. When the initial concentration increased further, the adsorbed active sites tended to be saturated [68].

3.3.4. Adsorption Kinetics

To investigate the effect of RIR/AA-co-AM on the adsorption rate, a kinetic model was used to fit the experimental data. For solid-liquid interactions, the most common kinetic models are pseudo-first-order as in Equation (3), and pseudo-second-order models as in Equation (4). The pseudo-first-order kinetic model assumes that the adsorption rate is controlled by diffusion and mass transfer, while the pseudo-second-order model assumes that chemisorption is the rate-controlling step [69].

$$\log(q_{e1} - q_t) = \log q_{e1} - \frac{k_1}{2.303} t \tag{4}$$

$$\frac{\mathrm{t}}{q_t} = \frac{1}{k_2 {q_{e2}}^2} + \frac{t}{q_{e2}} \tag{5}$$

where q_{e1} and q_{e2} (mg/g) are the equilibrium adsorption capacity, q_t (mg/g) the adsorption capacity at a specific time, k_1 (min^{-1}) and k_2 (g/mg*min) quasi-first-order and pseudo-second-order rate constant, respectively.

Figure 10 and Table 1 show the fitting curves and fitting parameters of the pseudo-first-order model and pseudo-second-order model. Table 1 shows that in the pseudo-first-order calculation, the calculated value (q_{e1}) did not match the experimental value, but the pseudo-second-order q_{e2} was closer to the experimental data. Consistent with this, the pseudo-second-order correlation coefficient (R^2) was high. The results showed that the pseudo-second-order kinetic equation better described the adsorption of heavy metal ions by the hydrogel, i.e., chemisorption was dominant. Additionally, the chemisorption rate of the reaction was proportional to the square of the unoccupied adsorption sites.

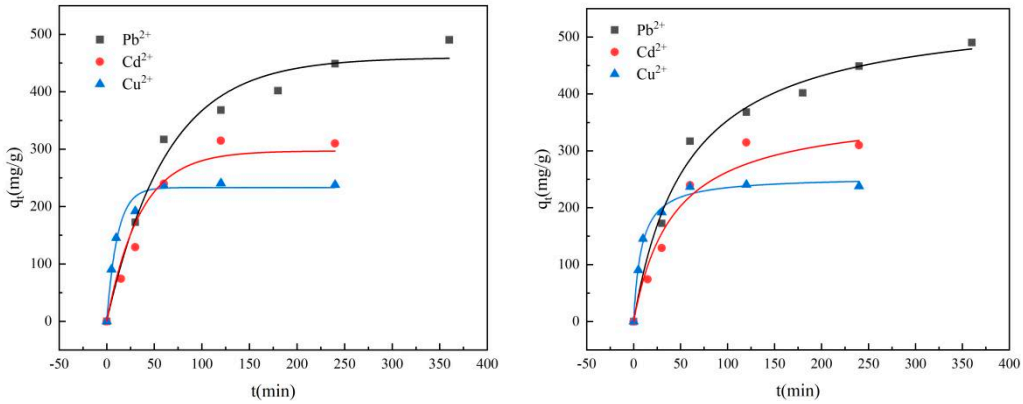

Figure 10. Pseudo-first-order (**a**), pseudo-second-order (**b**) kinetic model on heavy metal ions adsorption.

Table 1. Kinetic parameters for the adsorption of heavy metal ions.

	Pseudo-First-Order			**Pseudo-Second-Order**		
	k_1	q_{e1}	R^2	k_2	q_{e2}	R^2
Pb(II)	0.016	459.60	0.9747	0.00003	555.17	0.9867
Cd(II)	0.029	296.87	0.9583	0.00005	374.23	0.9627
Cu(II)	0.09	233.11	0.9800	0.00005	254.8	0.9910

3.3.5. Adsorption Isotherm

Adsorption isotherms are used to describe interfacial adsorption, a physicochemical adsorption phenomenon that results from the interaction of metal ions with the adsorbent surface. The Langmuir [70] and Freundlich [71] isotherm models were studied for the adsorption capacity of RIR/AA-co-AM. The Langmuir model was applied to a monolayer adsorption system, indicating that a limited number of adsorption sites were separated

from each other without chemical interactions. The Freundlich model described the non-uniform surface of the adsorption surface and was suitable for multi-layer adsorption or high adsorption concentration system. The equations were as follows:

$$\frac{C_e}{q_e} = \frac{1}{K_L q_m} + \frac{C_e}{q_m} \left\{ R_L = \frac{1}{1 + K_L C_0} \right\} \quad (6)$$

$$\ln q_e = \ln K_F + \frac{1}{n} \ln C_e \quad (7)$$

where q_e (mg/g) is the equilibrium adsorption capacity, C_e (mg/L) is the equilibrium concentration, K_L is the Langmuir constant, q_m (mg/g) is the maximum adsorption capacity covering the entire surface, R_L is the separation coefficient or equilibrium parameter, C_0 (mg/L) is the initial concentration of heavy metal ions, and K_F and n are the Freundlich constants.

Figure 11 and Table 2 describe the fitting parameters and fitting curves of the two models, respectively. According to the correlation coefficient (R^2), Langmuir was the best fitting method to describe the adsorption process, indicating that monolayer adsorption dominates the adsorption process. In addition, R_L values less than 1 and $n > 1$ both reflected the good adsorption capacity of the adsorbents.

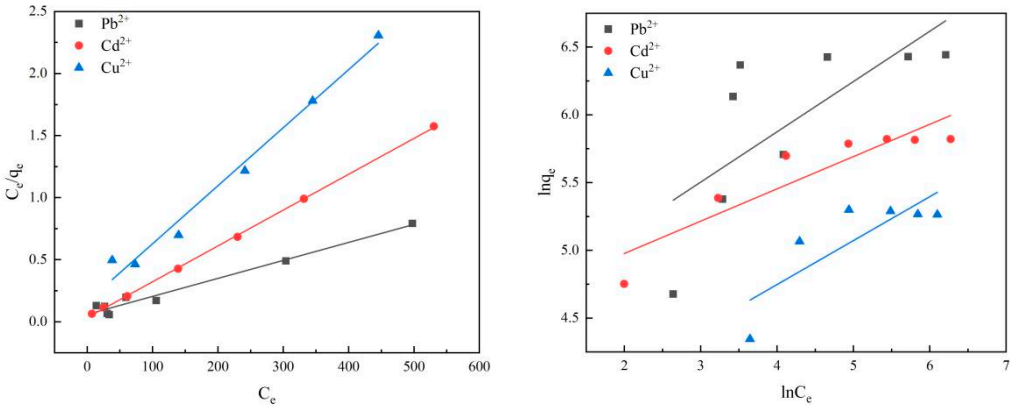

Figure 11. Langmuir (**a**), Freundlich (**b**) isotherm models of heavy metal ions adsorption on RIR/AA-co-AM.

Table 2. Adsorption isotherms of heavy metal ions on RIR/AA-co-AM hydrogel.

	Langmuir				**Freundlich**		
	q_m	K_L	R_L	R^2	n	K_F	R^2
Pb(II)	689.65	0.0244	0.0639	0.9745	2.695	80.654	0.5151
Cd(II)	346.02	0.0879	0.0222	0.9997	4.196	90.021	0.8328
Cu(II)	213.68	0.0292	0.1025	0.9828	3.085	31.521	0.6722

3.4. Adsorption Mechanism of Hydrogel

With the initiator, some weaker bonds were introduced into the cellulose macromolecules, so that the covalent bonds (C-C, C-O, C-H, O-H) with large bond energy in the cellulose molecules were broken. At the general polymerization temperature, primary free radicals that can initiate the graft copolymerization of monomers were generated on the cellulose molecules, and then free radical graft polymerization occurs [72]. The adsorption typically occurs through different interactions, which are extensively dependent on the functional groups present in the hydrogel, its properties, the chemical composition of pollutants, and experimental parameters [73]. The most common adsorption mechanism for the removal of heavy metals by adsorbents is electrostatic interactions [59]. Electrostatic

interaction comprised the interaction between charged modules, attractive and repulsive interaction occurred when molecules were oppositely charged (cation–anion interactions) and similarly charged (cation–cation or anion–anion interactions), respectively. The possible adsorption mechanism of RIR/AA-co-AM is shown in Figure 12. In this study, when pH was low but higher than 1, RIR/AA-co-AM deprotonated, the adsorbent functional groups -COOH, -$CONH_2$ and -OH could negatively charge, which was the opposite charge to the pollutants Pb^{2+}, Cd^{2+}, and Cu^{2+}, removing the pollutants by electrostatic interactions. In addition, functional groups -COOH, -$CONH_2$ were positively charged when pH was higher but below 5, which caused cations (Pb^{2+}, Cd^{2+}, and Cu^{2+}) exchange to remove the contaminants from wastewater.

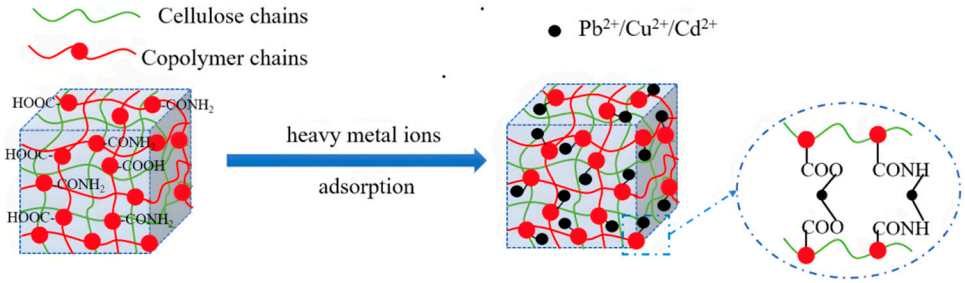

Figure 12. Ion exchange and electrostatic interactions mechanism.

Compared with the adsorbents reported in literature, the hydrogel prepared in this study has higher adsorption capacity for Pb^{2+}, Cd^{2+}, and Cu^{2+}, especially the adsorption of Pb^{2+} is higher than that of most adsorbents reported in the literature (Table 3). RIR/AA-co-AM showed a better adsorption capacity when compared to pure cellulose-synthesized MCC-g-poly(AA-co-AM), Ch/IA/MAA, GO/PAA, KCTS/PAM and SR–PAA introducing only monomeric AA or AM. Moreover, the preparation of these hydrogels all require heating during the synthesis process, increasing the synthesis costs. Furthermore, the RIR/AA-co-AM was prepared using natural by-product which could pollute groundwater if not utilized or disposed properly. RIR/AA-co-AM will not only alleviate the environmental pollution stress, but also improve the reutilization of Chinese herb residues. Therefore, Chinese herb residue based hydrogel synthesized in this study has a simple synthesis process and a relatively high adsorption capacity, which can serve as a more accessible and environmentally friendly adsorbent to remove heavy metal ions in wastewater.

Table 3. Adsorption of heavy metal ions by different adsorbents.

Adsorbent	Adsorption Capacity (mg/g)			References
	Pb^{2+}	Cd^{2+}	Cu^{2+}	
RIR/AA-co-AM	655.38	337.16	242.79	Present study
LR-NaOH	-	-	43.65	[16]
MCC-g-poly(AA-co-AM)	393.28	289.97	157.51	[7]
SR–PAA	422.69	160.75	-	[52]
Ch/IA/MAA	-	285.7	-	[62]
GO/PAA	-	316.4	-	[74]
KCTS/PAM	61.41	-	72.39	[75]

4. Limitations

Because the desorption performance of RIR/AA-co-AM was poor, the reusability experiment was not completed in this paper. In the future, we would like to further use oxidation and other means to turn metal ions into an oxidized state, thereby realizing the recovery of metal ions and the degradation of adsorbents.

5. Conclusions

Hydrogel biosorbents that could adsorb heavy metal ions in water under different conditions were successfully prepared using acrylic acid, acrylamide, and Radix Isatidis residue. Through the physicochemical characterization of this sample, acrylic acid and acrylamide monomers were grafted successfully with cellulose. SEM showed that the hydrogel surface was rough, irregular, and porous. The swelling ratio of RIR/PAA_4 was 9240% which was higher than that of RIR/AA-co-AM (9064%). RIR/AA-co-AM has an adsorption capacity for different kinds of heavy metal ions, among which the adsorption effect of Pb^{2+} was better. The maximum adsorption capacity of RIR/AA-co-AM for Pb^{2+} can be over 400 mg/g within 120 min. After 120 min, RIR/AA-co-AM could continuously adsorb Pb^{2+}. The maximum adsorption capacity of RIR/AA-co-AM for Cd^{2+} ion adsorption was about 300mg/g within 120 min. The maximum adsorption capacity of RIR/AA-co-AM for Cu^{2+} ion adsorption was 242.79 mg/g in 120 min. Compared with RIR/PAA_4 and RIR/PAM_3, the overall adsorption capacity of RIR/AA-co-AM was higher. Moreover, the adsorption process of hydrogels for heavy metal ions was well described by the pseudo-second-order kinetic equation and Langmuir adsorption isotherm. The adsorption mechanism of RIR/AA-co-AM was identified as the electrostatic adsorption and ion-exchange effect. The results indicated that the prepared hydrogels were potential biosorbents for the removal of heavy metal ions from wastewater, providing a promising way for the preparation of biosorbents and cyclic utilization of Chinese herb residues further.

Author Contributions: Conceptualization, X.Y. and H.Z.; methodology, H.Z.; software, H.Z.; validation, X.Y., H.Z. and H.W.; formal analysis, H.Z.; investigation, X.Y.; resources, Y.G.; data curation, H.Z.; writing—original draft preparation, X.Y.; writing—review and editing, P.X.; visualization, T.K.; supervision, H.W.; project administration, X.Y.; funding acquisition, Y.G. All authors have read and agreed to the published version of the manuscript.

Funding: This work was supported by the Innovation Fund Project of Higher Education in Gansu Province (2021B-159), the Natural Science Foundation of Gansu Province (21JR1RA257), and the Talent Introduction Plan of Gansu University of Chinese Medicine (2018YJRC-10).

Data Availability Statement: The data presented in this study are available on request from the first author (X.Y.) and corresponding author (H.W.).

Conflicts of Interest: The authors declare no conflict of interest.

References

1. Richardson, J.R.; Fitsanakis, V.; Westerink RH, S.; Kanthasamy, A.G. Neurotoxicity of pesticides. *Acta Neuropathol.* **2019**, *138*, 343–362. [CrossRef] [PubMed]
2. Chandrabose, G.; Dey, A.; Gaur, S.S.; Pitchaimuthu, S.; Jagadeesan, H.; Braithwaite, N.S.J.; Selvaraj, V.; Kumar, V.; Krishnamurthy, S. Removal and degradation of mixed dye pollutants by integrated adsorption-photocatalysis technique using 2-D MoS_2/TiO_2 nanocomposite. *Chemosphere* **2021**, *279*, 130467–130478. [CrossRef] [PubMed]
3. Yan, C.; Qu, Z.; Wang, J.; Cao, L.; Han, Q. Microalgal bioremediation of heavy metal pollution in water: Recent advances, challenges, and prospects. *Chemosphere* **2022**, *286*, 131870. [CrossRef]
4. Komijani, M.; Shamabadi, N.S.; Shahin, K.; Eghbalpour, F.; Tahsili, M.R.; Bahram, M. Heavy metal pollution promotes antibiotic resistance potential in the aquatic environment. *Environ. Pollut.* **2021**, *274*, 116569. [CrossRef]
5. Li, X.; Shen, H.; Zhao, Y.; Cao, W.; Hu, C.; Sun, C. Distribution and Potential Ecological Risk of Heavy Metals in Water, Sediments, and Aquatic Macrophytes: A Case Study of the Junction of Four Rivers in Linyi City, China. *Int. J. Environ. Res. Public Health* **2019**, *16*, 2861. [CrossRef]
6. Liu, M.; Liu, Y.; Shen, J.; Zhang, S.; Liu, X.; Chen, X.; Ma, Y.; Ren, S.; Fang, G.; Li, S.; et al. Simultaneous removal of Pb^{2+}, Cu^{2+} and Cd^{2+} ions from wastewater using hierarchical porous polyacrylic acid grafted with lignin. *J. Hazard. Mater.* **2020**, *392*, 122208. [CrossRef] [PubMed]
7. Wang, Y.; Wang, B.; Wang, Q.; Di, J.; Miao, S.; Yu, J. Amino-Functionalized Porous Nanofibrous Membranes for Simultaneous Removal of Oil and Heavy-Metal Ions from Wastewater. *ACS Appl. Mater. Interfaces* **2018**, *11*, 1672–1679. [CrossRef]
8. Zhu, L.; Ji, J.; Wang, S.; Xu, C.; Yang, K.; Xu, M. Removal of Pb(II) from wastewater using Al_2O_3-NaA zeolite composite hollow fiber membranes synthesized from solid waste coal fly ash. *Chemosphere* **2018**, *206*, 278–284. [CrossRef]
9. Rehman, M.-U.; Rehman, W.; Waseem, M.; Hussain, S.; Haq, S.; Rehman, M.A. Adsorption mechanism of Pb^{2+} ions by Fe_3O_4, SnO_2, and TiO_2 nanoparticles. *Environ. Sci. Pollut. Res.* **2019**, *26*, 19968–19981. [CrossRef]

10. Joseph, L.; Jun, B.M.; Flora, J.R.V.; Park, C.M.; Yoon, Y. Removal of heavy metals from water sources in the developing world using low-cost materials: A review. *Chemosphere* **2019**, *229*, 142–159. [CrossRef]
11. Ali, I.; Peng, C.; Lin, D.; Saroj, D.P.; Naz, I.; Khan, Z.M.; Sultan, M.; Ali, M. Encapsulated green magnetic nanoparticles for the removal of toxic Pb^{2+} and Cd^{2+} from water: Development, characterization and application. *J. Environ. Manag.* **2018**, *234*, 273–289. [CrossRef] [PubMed]
12. Ye, L.; Wang, N.; Wang, S. Blood lead level of outpatient children in Anqing from 2015 to 2018. *Chin. J. Sch. Health* **2021**, *42*, 1548–1551. [CrossRef]
13. Darban, Z.; Shahabuddin, S.; Gaur, R.; Ahmad, I.; Sridewi, N. Hydrogel-Based Adsorbent Material for the Effective Removal of Heavy Metals from Wastewater: A Comprehensive Review. *Gels* **2022**, *8*, 263. [CrossRef] [PubMed]
14. Saxena, G.; Purchase, D.; Mulla, S.I.; Saratale, G.D.; Bharagava, R.N. Phytoremediation of Heavy Metal-Contaminated Sites: Eco-environmental Concerns, Field Studies, Sustainability Issues, and Future Prospects. In *Reviews of Environmental Contamination and Toxicology*; Springer: Cham, Switzerland, 2019; Volume 249, pp. 71–131. [CrossRef]
15. Zhao, B.; Jiang, H.; Lin, Z.; Xu, S.; Xie, J.; Zhang, A. Preparation of acrylamide/acrylic acid cellulose hydrogels for the adsorption of heavy metal ions. *Carbohydr. Polym.* **2019**, *224*, 115022. [CrossRef]
16. Yin, X.C.; Zhang, N.D.; Du, M.X.; Zhu, H.; Ke, T. Preparation of bio-absorbents by modifying licorice residue via chemical methods and removal of copper ions from wastewater. *Water Sci. Technol.* **2021**, *84*, 3528–3540. [CrossRef]
17. Zhan, Y.; Guan, X.; Ren, E.; Lin, S.; Lan, J. Fabrication of zeolitic imidazolate framework-8 functional polyacrylonitrile nanofibrous mats for dye removal. *J. Polym. Res.* **2019**, *26*, 145. [CrossRef]
18. Liu, X.; Tian, J.; Li, Y.; Sun, N.; Mi, S.; Xie, Y.; Chen, Z. Enhanced dyes adsorption from wastewater via Fe_3O_4 nanoparticles functionalized activated carbon. *J. Hazard. Mater.* **2019**, *373*, 397–407. [CrossRef]
19. Hua, J.; Meng, R.; Wang, T.; Gao, H.; Luo, Z.; Jin, Y.; Liu, L.; Yao, J. Highly Porous Cellulose Microbeads and their Adsorption for Methylene Blue. *Fibers Polym.* **2019**, *20*, 794–803. [CrossRef]
20. Yang, S.C.; Liao, Y.; Karthikeyan, K.G.; Pan, X.J. Mesoporous cellulose-chitosan composite hydrogel fabricated via the co-dissolution-regeneration process as biosorbent of heavy metals. *Environ. Pollut.* **2021**, *286*, 117324–117333. [CrossRef]
21. Yan, R.R.; Gong, J.S.; Su, C.; Liu, Y.L.; Qian, J.Y.; Xu, Z.H.; Shi, J.S. Preparation and applications of keratin biomaterials from natural keratin wastes. *Appl. Microbiol. Biotechnol.* **2022**, *106*, 2349–2366. [CrossRef]
22. Yin, X.C.; Li, F.Y.; He, Y.F.; Wang, Y.; Wang, R.M. Study on effective extraction of chicken feather keratins and their films for controlling drug release. *Biomater. Sci.* **2013**, *1*, 528–536. [CrossRef] [PubMed]
23. Ren, J.M.; Wu, S.W. *The Application of Nature Absorbents for Heavy Metals Uptake from Contaminated Water*; Chongqing Technol Business University (NatSciEd): Chongqing, China, 2005; pp. 537–540.
24. Shi, Y.Z.; Yin, X.C.; Si, G.H.; Zhang, N.D.; Du, M.X.; Wang, X.H. Bio-adsorbent preparation based on Chinese radix isatidis residue for Pb(II) removal. *Water Pract. Technol.* **2020**, *15*, 1202–1212. [CrossRef]
25. Huang, Y.; Meng, F.; Liu, R.; Yu, Y.; Yu, W. Morphology and supramolecular structure characterization of cellulose isolated from heat-treated moso bamboo. *Cellulose* **2019**, *26*, 7067–7078. [CrossRef]
26. Wittmar AS, M.; Baumert, D.; Ulbricht, M. Cotton as Precursor for the Preparation of Porous Cellulose Adsorbers. *Macromol. Mater. Eng.* **2021**, *306*, 2000778. [CrossRef]
27. Qin, Q.; Guo, R.; Lin, S.; Jiang, S.; Lan, J.; Lai, X.; Cui, C.; Xiao, H.; Zhang, Y. Waste cotton fiber/Bi_2WO_6 composite film for dye removal. *Cellulose* **2019**, *26*, 3909–3922. [CrossRef]
28. Liu, Q.; He, W.Q.; Aguedo, M.; Xia, X.; Bai, W.B.; Dong, Y.Y.; Song, J.Q.; Richel, A.; Goffin, D. Microwave-assisted alkali hydrolysis for cellulose isolation from wheat straw: Influence of reaction conditions and non-thermal effects of microwave. *Carbohydr. Polym.* **2020**, *253*, 117170–117199. [CrossRef]
29. Meez, E.; Rahdar, A.; Kyzas, G. Sawdust for the Removal of Heavy Metals from Water: A Review. *Molecules* **2021**, *26*, 4318. [CrossRef]
30. Qamouche, K.; Chetaine, A.; El Yahyaoui, A.; Moussaif, A.; Fröhlich, P.; Bertau, M.; Haneklaus, N. Uranium and other heavy metal sorption from Moroccan phosphoric acid with argan nutshell sawdust. *Miner. Eng.* **2021**, *171*, 107085. [CrossRef]
31. Phitsuwan, P.; Sakka, K.; Ratanakhanokchai, K. Structural changes and enzymatic response of Napier grass (*Pennisetum purpureum*) stem induced by alkaline pretreatment. *Bioresour. Technol.* **2016**, *218*, 247–256. [CrossRef]
32. Huang, L.J.; Lee, W.J.; Chen, Y.C. Bio-Based Hydrogel and Aerogel Composites Prepared by Combining Cellulose Solutions and Waterborne Polyurethane. *Polymers* **2022**, *14*, 204. [CrossRef]
33. Liu, G.; Huang, Y.; Xu, L. Biochar from Chinese herb residues as adsorbent for toxic metals removal. *IOP Conf. Ser. Earth Environ. Sci.* **2017**, *61*, 12147. [CrossRef]
34. Yang, L.; Xia, L.H.; Zhang, Z.H.; Zu, Y.G. Present situation and development trend of eco-utilization of residue production in plant extraction. *Mod. Chem. Ind.* **2008**, *28*, 14–17. [CrossRef]
35. Guo, F.; Dong, Y.; Dong, L.; Jing, Y. An innovative example of herb residues recycling by gasification in a fluidized bed. *Waste Manag.* **2013**, *33*, 825–832. [CrossRef] [PubMed]
36. Zhao, S.; Zhou, T. Biosorption of methylene blue from wastewater by an extraction residue of *Salvia miltiorrhiza* Bge. *Bioresour. Technol.* **2016**, *219*, 330–337. [CrossRef]
37. Feng, N.; Zhang, F. Untreated Chinese ephedra residue as biosorbents for the removal of Pb^{2+} ions from aqueous solutions. *Procedia Environ. Sci.* **2013**, *18*, 794–799. [CrossRef]

38. Xue, Y.T.; Du, C.F.; Wu, Z.H.; Zhang, L.H. Relationship of the cellulose and lignin contents in biomass to the structure and RB-19 adsorption behavior on activated carbon. *New J. Chem.* **2018**, *42*, 16493–16502. [CrossRef]
39. Teow, Y.H.; Kam, L.M.; Mohammad, A.W. Synthesis of cellulose hydrogel for copper (II) ions adsorption. *J. Environ. Chem. Eng.* **2018**, *6*, 4588–4597. [CrossRef]
40. Shalla, A.H.; Yaseen, Z.; Bhat, M.A.; Rangreez, T.A.; Maswal, M. Recent review for removal of metal ions by hydrogels. *Sep. Sci. Technol.* **2019**, *54*, 89–100. [CrossRef]
41. Lu, J.; Chen, Y.; Ding, M.; Fan, X.; Hu, J.; Chen, Y.; Li, J.; Li, Z.; Liu, W. A 4arm-PEG macromolecule crosslinked chitosan hydrogels as antibacterial wound dressing. *Carbohydr. Polym.* **2022**, *277*, 118871. [CrossRef]
42. Chen, Y.; Li, J.; Lu, J.; Ding, M.; Chen, Y. Synthesis and properties of Poly(vinyl alcohol) hydrogels with high strength and toughness. *Polym. Test.* **2022**, *108*, 107516. [CrossRef]
43. Ozay, O.; Ekici, S.; Baran, Y.; Kubilay, S.; Aktas, N.; Sahiner, N. Utilization of magnetic hydrogels in the separation of toxic metal ions from aqueous environments. *Desalination* **2010**, *260*, 57–64. [CrossRef]
44. Jang, S.H.; Jeong, Y.G.; Gil Min, B.; Lyoo, W.S.; Lee, S.C. Preparation and lead ion removal property of hydroxyapatite/polyacrylamide composite hydrogels. *J. Hazard. Mater.* **2008**, *159*, 294–299. [CrossRef]
45. Dai, L.; Cheng, T.; Xi, X.; Nie, S.; Ke, H.; Liu, Y.; Tong, S.; Chen, Z. A versatile TOCN/CGG self-assembling hydrogel for integrated wastewater treatment. *Cellulose* **2020**, *27*, 915–925. [CrossRef]
46. Godiya, C.B.; Cheng, X.; Li, D.; Chen, Z.; Lu, X. Carboxymethyl cellulose/polyacrylamide composite hydrogel for cascaded treatment/reuse of heavy metal ions in wastewater. *J. Hazard. Mater.* **2019**, *364*, 28–38. [CrossRef] [PubMed]
47. Ozay, O.; Ekici, S.; Baran, Y.; Aktas, N.; Sahiner, N. Removal of toxic metal ions with magnetic hydrogels. *Water Res.* **2009**, *43*, 4403–4411. [CrossRef] [PubMed]
48. Maijan, P.; Junlapong, K.; Arayaphan, J.; Khaokong, C.; Chantarak, S. Synthesis and characterization of highly elastic superabsorbent natural rubber/polyacrylamide hydrogel. *Polym. Degrad. Stab.* **2021**, *186*, 109499. [CrossRef]
49. Zainal, S.H.; Mohd, N.; Suhaili, N.; Anuar, F.H.; Lazim, A.M.; Othaman, R. Preparation of cellulose-based hydrogel: A review. *J. Mater. Res. Technol.* **2021**, *10*, 935–952. [CrossRef]
50. Akter, M.; Bhattacharjee, M.; Dhar, A.K.; Rahman, F.B.A.; Haque, S.; Rashid, T.U.; Kabir, S.M.F. Cellulose-Based Hydrogels for Wastewater Treatment: A Concise Review. *Gels* **2021**, *7*, 30. [CrossRef]
51. Javed, R.; Shah, L.A.; Sayed, M.; Khan, M.S. Uptake of heavy metal ions from aqueous media by hydrogels and the irconversion to nanoparticles for generation of a catalyst system: Two-fold application study. *RSC Adv.* **2018**, *8*, 14787–14797. [CrossRef]
52. Hosseinzadeh, H.; Barghi, A. Synthesis of poly(AN)/poly(AA-co-AM) hydrogel nanocomposite with electrical conductivity and antibacterial properties. *Polym. Compos.* **2018**, *40*, 2724–2733. [CrossRef]
53. Huang, S.; Wang, X.; Shen, J.; Wu, R.; Zhao, H.; Wang, Y.; Wang, Y.; Xia, Y. Surface functionalization of cellulose nanocrystals with polymeric ionic liquids during phase transfer. *Carbohydr. Polym.* **2017**, *157*, 1426–1433. [CrossRef]
54. Chen, H.; Shao, J. Analysis of Polyaeryamide by Infrared Spectroscopy. *Anal. Instrum.* **2011**, *3*, 36–40. [CrossRef]
55. Zhang, M.; Zhang, S.; Chen, Z.; Wang, M.; Cao, J.; Wang, R. Preparation and Characterization of Superabsorbent Polymers Based on Sawdust. *Polymers* **2019**, *11*, 1891. [CrossRef]
56. Ali, A.E.H. Removal of heavy metals from model wastewater by using carboxymehyl cellulose/2-acrylamido-2-methyl propane sulfonic acid hydrogels. *J. Appl. Polym. Sci.* **2012**, *123*, 763–769. [CrossRef]
57. Ge, D.; Yuan, H.; Xiao, J.; Zhu, N. Insight into the enhanced sludge dewaterability by tannic acid conditioning and pH regulation. *Sci. Total Environ.* **2019**, *679*, 298–306. [CrossRef]
58. Bai, B.; Bai, F.; Li, X.; Nie, Q.; Jia, X.; Wu, H. The remediation efficiency of heavy metal pollutants in water by industrial red mud particle waste. *Environ. Technol. Innov.* **2022**, *28*, 102944. [CrossRef]
59. Peng, X.; Zheng, J.; Liu, Q.; Hu, Q.; Sun, X.; Li, J.; Liu, W.; Lin, Z. Efficient removal of iron from red gypsum via synergistic regulation of gypsum phase transformation and iron speciation. *Sci. Total Environ.* **2021**, *791*, 148319. [CrossRef]
60. Badsha, M.A.; Khan, M.; Wu, B.; Kumar, A.; Lo, I.M.C. Role of surface functional groups of hydrogels in metal adsorption: From performance to mechanism. *Hazard. Mater.* **2021**, *408*, 124463. [CrossRef]
61. Badsha, M.A.; Lo, I.M. An innovative pH-independent magnetically separable hydrogel for the removal of Cu(II) and Ni(II) ions from electroplating wastewater. *Hazard. Mater.* **2020**, *381*, 121000. [CrossRef]
62. Milosavljević, N.B.; Ristić, M.Đ.; Perić-Grujić, A.A.; Filipović, J.M.; Štrbac, S.B.; Rakočević, Z.L.; Kalagasidis Krušić, M.T. Hydrogel based on chitosan, itaconic acid and methacrylic acid as adsorbent of Cd^{2+} ions from aqueous solution. *Chem. Eng. J.* **2010**, *165*, 554–562. [CrossRef]
63. Akpomie, K.G.; Dawodu, F.A.; Adebowale, K.O. Mechanism on the sorption of heavy metals from binary-solution by a low cost montmorillonite and its desorption potential. *Alex. Eng. J.* **2015**, *54*, 757–767. [CrossRef]
64. Wong, S.; Ghafar, N.A.; Ngadi, N.; Razmi, F.A.; Inuwa, I.M.; Mat, R.; Amin, N.A.S. Effective removal of anionic textile dyes using adsorbent synthesized from coffee waste. *Sci. Rep.* **2020**, *10*, 2928–2940. [CrossRef]
65. Chen, X.; Zhou, S.; Zhang, L.; You, T.; Xu, F. Adsorption of heavy metals by graphene oxide/cellulose hydrogel prepared from NaOH/urea aqueous solution. *Materials* **2016**, *9*, 582. [CrossRef]
66. Abdelwahab, H.E.; Hassan, S.Y.; Mostafa, M.A.; El Sadek, M.M. Synthesis and characterization of glutamic-chitosan hydrogel for copper and nickel removal from wastewater. *Molecules* **2016**, *21*, 684. [CrossRef]

67. Kabir, S.F.; Sikdar, P.P.; Haque, B.; Bhuiyan, M.R.; Ali, A.; Islam, M. Cellulose-based hydrogel materials: Chemistry, properties and their prospective applications. *Prog. Biomater.* **2018**, *7*, 153–174. [CrossRef]
68. Chen, Y.; Chen, Q.; Zhao, H.; Dang, J.; Jin, R.; Zhao, W.; Li, Y. Wheat straws and corn straws as adsorbents for the removal of Cr(VI) and Cr(III) from aqueous solution: Kinetics, isotherm, and mechanism. *ACS Omega* **2020**, *5*, 6003–6009. [CrossRef]
69. Chen, Q.; Zheng, J.; Zheng, L.; Dang, Z.; Zhang, L. Classical theory and electron-scale view of exceptional Cd adsorption onto mesoporous cellulose biochar via experimental analysis coupled with DFT calculations. *Chem. Eng. J.* **2018**, *350*, 1000–1009. [CrossRef]
70. Nongbe, M.C.; Bretel, G.; Ekou, T.; Ekou, L.; Yao, B.K.; Le Grognec, E.; Felpin, F.X. Cellulose paper grafted with polyamines as powerful adsorbent for heavy metals. *Cellulose* **2018**, *25*, 4043–4055. [CrossRef]
71. Hamdaoui, O.; Naffrechoux, E. Modeling of adsorption isotherms of phenol and chlorophenols onto granular activated carbon: Part, I. Two-parameter models and equations allowing determination of thermodynamic parameters. *J. Hazard. Mater.* **2007**, *147*, 381–394. [CrossRef]
72. Song, R.Z.; Chen, Y.F.; Pan, H.S.; Zeng, M.Z. Graft Copolymerization of Acrylic Acid onto Superfine Cellulose. *Cellul. Sci. Technol.* **2001**, *4*, 11–15+20. [CrossRef]
73. Sinha, V.; Chakma, S. Advances in the preparation of hydrogel for wastewater treatment: A concise review. *J. Environ. Chem. Eng.* **2019**, *7*, 103295. [CrossRef]
74. Kong, W.; Yue, Q.; Li, Q.; Gao, B. Adsorption of Cd^{2+} on GO/PAA hydrogel and preliminary recycle to GO/PAA-CdS as efficient photocatalyst. *Sci. Total Environ.* **2019**, *668*, 1165–1174. [CrossRef] [PubMed]
75. Zhao., Z.; Huang, Y.; Wu, Y.; Li, S.; Yin, H.; Wang, J. α-ketoglutaric acid modified chitosan/polyacrylamide semi-interpenetrating polymer network hydrogel for removal of heavy metal ions. *Colloids Surf. Physicochem. Eng. Asp.* **2021**, *628*, 127262. [CrossRef]